J Plant Res (2010) 123:421–432
DOI 10.1007/s10265-010-0310-0

Estimating stem volume and biomass of *Pinus koraiensis* using LiDAR data

Doo-Ahn Kwak · Woo-Kyun Lee · Hyun-Kook Cho · Seung-Ho Lee · Yowhan Son · Menas Kafatos · So-Ra Kim

Received: 31 July 2009 / Accepted: 12 December 2009 / Published online: 25 February 2010

Abstract The objective of this study was to estimate the stem volume and biomass of individual trees using the crown geometric volume (CGV), which was extracted from small-footprint light detection and ranging (LiDAR) data. Attempts were made to analyze the stem volume and biomass of Korean Pine stands (*Pinus koraiensis* Sieb. et Zucc.) for three classes of tree density: low (240 N/ha), medium (370 N/ha), and high (1,340 N/ha). To delineate individual trees, extended maxima transformation and watershed segmentation of image processing methods were applied, as in one of our previous studies. As the next step, the crown base height (CBH) of individual trees has to be determined; information for this was found in the LiDAR point cloud data using *k*-means clustering. The LiDAR-derived CGV and stem volume can be estimated on the basis of the proportional relationship between the CGV and stem volume. As a result, low tree-density plots had the best performance for LiDAR-derived CBH, CGV, and stem volume ($R^2 = 0.67$, 0.57, and 0.68, respectively) and accuracy was lowest for high tree-density plots ($R^2 = 0.48$, 0.36, and 0.44, respectively). In the case of medium tree-density plots accuracy was $R^2 = 0.51$, 0.52, and 0.62, respectively. The LiDAR-derived stem biomass can be predicted from the stem volume using the wood basic density of coniferous trees (0.48 g/cm^3), and the LiDAR-derived above-ground biomass can then be estimated from the stem volume using the biomass conversion and expansion factors (BCEF, 1.29) proposed by the Korea Forest Research Institute (KFRI).

Keywords Above-ground biomass · Crown base height · Crown geometric volume · *k*-means clustering · LiDAR · Stem volume

Introduction

Concerns about global climate change have highlighted the importance of finding efficient ways of quantifying terrestrial carbon stocks on regional, landscape, and global scales (Boudreau et al. 2008). Quantifying carbon storage is important in understanding the carbon cycle (Malhi et al. 2002). Measurement of forest biomass provides an indication of carbon sequestration in trees (Popescu 2007), because the amount of carbon stock in forested areas can be evaluated from forest biomass and soil carbon sinks. Moreover, the stem volume is also essential information for measuring forest biomass because the biomass is converted from volume information. Above-ground biomass is generally estimated on the basis of field survey, which provides a consistent means of assessing biomass. However, it is a very intensive, time-consuming, and costly work to acquire information on individual trees with limited geographic coverage (Kwak et al. 2007).

Electronic supplementary material The online version of this article (doi:10.1007/s10265-010-0310-0) contains supplementary material, which is available to authorized users.

D.-A. Kwak · W.-K. Lee (✉) · Y. Son · S.-R. Kim
Division of Environmental Science and Ecological Engineering, Korea University, Seoul 136-701, South Korea
e-mail: leewk@korea.ac.kr

H.-K. Cho · S.-H. Lee
Division of Forest Resources Information, Korea Forest Research Institute, Seoul 136-012, South Korea

M. Kafatos
Center of Excellence in Earth Observing, Schmid College of Science, Chapman University, Orange, CA 92866, USA

To solve such problems, several studies have tried to evaluate the possibility of using remotely sensed data acquired by use of optical sensors. The remote sensing technique is relatively low cost, and makes it possible to obtain measurements from every location, including inaccessible areas, and to collect and process data quickly (Bortolot and Wynne 2005). However, it is difficult to obtain the three-dimensional information on forests required for estimating biomass, for example tree height, crown base height, and CGV, directly from optical sensors.

To overcome these drawbacks, the light detection and ranging (LiDAR) technique has recently been used to extract surface information, because it can acquire highly accurate object-shape characteristics using geo-registered three-dimensional (x, y, z) mass points (Kwak et al. 2007). LiDAR systems are active remote-sensing devices which measure the time taken by laser pulses sent from an airborne LiDAR system to reach the ground and be reflected back to the sensor (Popescu 2007). The measured time is converted into a distance between the LiDAR system and the object on the ground, i.e. LiDAR systems convert time data into spatial data. The converted distance is used for precise three-dimensional characterization of reflecting ground surfaces. Therefore, both vertical and horizontal forest structures in forest vegetation, for example tree heights, sub-canopy topographies, and distributions required for estimating tree volumes and biomass can be measured with high precision (Holmgren et al. 2003).

There are two LiDAR systems for acquiring three-dimensional information on forest vegetation. The major factors distinguishing between these LiDAR systems are the footprint size of the laser beam and the record of backscatter intensity (Bortolot and Wynne 2005). The footprint size of the laser beam is a general criterion by which LiDAR systems are classified into two categories: large or small-footprint. Large-footprint LiDAR systems have a laser footprint diameter of more than 5 m whereas small-footprint LiDAR systems have a narrow beam diameter of less than 50 cm. Another criterion is the type of recording laser beam used to measure intensity. Large-footprint LiDAR systems can record continuous wave forms along a single track defined by the flight line, and operate on the assumption that the shape of the waveform from the returned signal represents a vertical distribution of the intercepted surfaces within a given laser footprint (Fig. S1).

On the other hand, small-footprint LiDAR systems record discrete signals, not continuous information about vertical forest structure (Fig. S2; Nelson et al. 1988, 2004; Naesset 1997; Hyyppä and Inkinen 1999; Lefsky et al. 1999a, b, 2001, 2002; Means et al. 1999; Drake et al. 2002, 2003; Lim et al. 2003; Popescu et al. 2003, 2004; Lim and Treitz 2004). Discrete returns can yield valuable information, for example biophysical information of individual trees, because of their high spatial resolution, as mentioned above (Morsdorf et al. 2005). However, large-footprint LiDAR systems cannot provide precise information because of their larger footprint size and coarse spacing (Van Aardt 2004). Thus, large-footprint LiDAR systems may be suitable for investigations at the plot or stand level. In this study, attempts were made to extract biomass information at the individual tree level using LiDAR data acquired from a small-footprint LiDAR system (ALTM 3070 by Optech, Canada).

Previous LiDAR studies of stem volumes or biomass, whether using large or small-footprint LiDAR systems, attempted to derive tree heights and crown dimensions, and then use allometric relationships to estimate the biomass at the plot or individual tree level. In particular, estimation of biomass has been performed in South Korea using an allometric equation: $\text{Biomass} = f(\text{TH}, \text{DBH})$, which is based on the field-derived quantities tree height (TH) and diameter at breast height (DBH) (Kim et al. 2000). The tree height can be extracted relatively easily from satellite imagery, aerial photos, and LIDAR data via a stereo analysis or with independent imagery, whereas the DBH cannot be estimated directly from remotely sensed data, including LiDAR data (Hyyppä et al. 2001; Shimada et al. 2001; Persson et al. 2002; Brandtberg et al. 2003; Leckie et al. 2003; Popescu et al. 2003; Popescu and Wynne 2004; Kubo et al. 2007, Kwak et al. 2007). Therefore, an additional allometric relationship: $\text{DBH} = f(\text{Crown Diameter})$, between the field-derived DBH and crown diameter must be regressed in order to estimate the forest biomass using remotely sensed data. Namely, the forest biomass must have been estimated using two such modeling processes if remotely sensed data are used. To avoid complicated processes and to approximate the real biomass; in particular, a method for calculating stem volume and biomass was developed using only crown geometric volumes (CGVs), defined as the crown volume above the crown base height extracted from LiDAR data (Chen et al. 2007).

To estimate the CGV, isolation of individual trees has to be initially carried out. With the high pulse-density of small-footprint LiDAR data, it has recently been shown possible to isolate individual trees and directly extract individual tree properties, including treetop locations, tree heights, crown width, crown boundaries, and the CGV (Popescu et al. 2003; Hyyppä et al. 2001; Persson et al. 2002, Kwak et al. 2007). A new method was also developed to delineate individual tree crowns in Korean Pine, Japanese Larch, and Oak stands in central Korea using small-footprint LiDAR data (Kwak et al. 2007).

The objectives of this study were:

1. to estimate stem volume from the CGV based on individual trees to accompany our previous study on the delineation of individual trees; and
2. to compute above-ground biomass by converting the stem volume using the biomass conversion and expansion factors (BCEF) developed by the Korea Forest Research Institute (KFRI).

Materials

Study area

The study area was located in Gwangneung Experimental Forest of the Korea Forest Research Institute (datum: Geodetic Reference System 1980 (GRS80), Coordinates: upper left 127°09′25.864″E, 37°45′46.265″N and lower right 127°10′44.629″E, 37°44′10.201″E), central South Korea (Fig. 1). Approximately 80 ha of private forests were selected as the study area, which ranged from 160 to 573 m above sea level and was dominated by steep hills, with the main tree species being Japanese Red Pine (*Pinus densiflora*), Korean Pine (*Pinus koraiensis*), Japanese Larch (*Larix leptolepis*), and Oaks (*Quercus* spp.). For this study, Korean Pine stands were selected and five plots investigated. These stands were selected in such a way that the composition of tree species was homogeneous.

Acquisition of LiDAR data and ground data

An Optech ALTM 3070 (a small-footprint LiDAR system) was used to acquire the LiDAR data. The flight was performed on 3rd April, 2007. The study area was measured at an altitude of 1,400 m, with a sampling density of 5–10 points per square meter, and radiometric resolution, scan frequency, scan width, and beam divergence of 12 bits, 70 Hz, ±20°, and 0.31 mrad, respectively.

The field survey was performed from 11th to 15th May, 2009. Sample sites were composed of five plots of Korean Pine, each with an area of 0.05 ha ($r = 12.7$ m) and 50-year-old stands (even-aged stands). The five plots investigated were classified into three categories according to their tree density: high (1,340 N/ha), medium (370 N/ha), and low (240 N/ha) tree-density plots. The reason for this was that the overlapping crown areas between neighbor trees is determined by the tree density, and factors such as tree height, DBH, and crown width are affected by the growing space (Tange et al. 1994). The tree height, DBH, crown base height, crown width, and positions of individual trees were measured to obtain basic information on the sample plots (Table S1).

The positions of the individual trees were acquired at the breast height of the trees, using a GPS Pathfinder Pro XR, manufactured by Trimble. To correct positional errors in the plots surveyed using a single GPS receiver, the GPS data were processed by differential correction using information for correcting positioning errors caused by the clocks in satellites and receivers, the atmosphere, satellite orbits, and reflective surfaces near the receiver. The information was received from a GPS continuous station near the study area, which acquires precise position and error correction information every 30 s (Lee et al. 2003). The positions of correctly geo-referenced plots were; thereby, obtained with positional errors within 1 m.

Ground data were obtained between 11th and 15th May 2009, although the LiDAR data were acquired on 3rd April 2007. However, differences in the tree height, DBH, crown base height, and crown width growth relevant to the period between acquisition of the ground data and the LiDAR-derived values was not considered, because the changes in

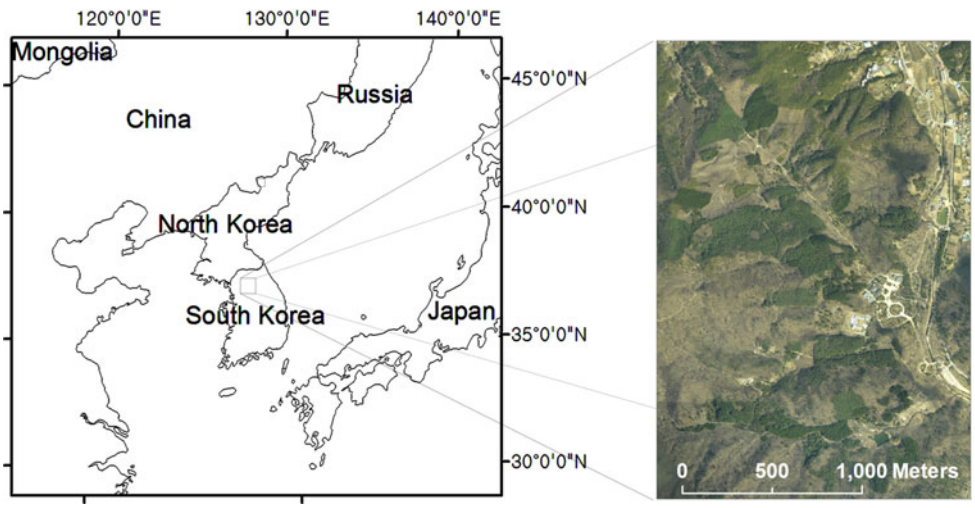

Fig. 1 Digital aerial photograph of the study area acquired on 3 April 2007. Coniferous trees of the area are composed of Japanese Red Pine (*Pinus densiflora*), Korean Pine (*Pinus koraiensis*), and Needle Fir (*Abies holophylla*)

these factors over the 2-year period were judged to be relatively small.

Methods

Classification of LiDAR data and derivation of CHM

In order to generate a digital terrain model (DTM), digital surface model (DSM), and crown height model (CHM), the LiDAR data were classified into two groups: ground returns and canopy returns. Ground returns are LiDAR returns reflected by the ground, which were extracted using the TerraScan software's automatic procedure. The CHM was computed by subtracting the DTM, as a representation of the ground area, from the DSM, as a representation of the surface of the crowns. Because the along-track distances were longer than those across-track (Fig. S3a), there was the potential for the surface models to contain false strips in the flying direction, which are caused by the precipitous difference between neighboring cells (Kwak et al. 2007). A narrower distance between LiDAR returns will allow less difference between interpolated cells in the generated raster data such as DCM and DSM. In order to cope with this problem, canopy returns were filtered with a 0.3 m × 0.3 m window to select only the highest points within the window, with these filtered points used to generate the DTM and CHM (Fig. S3b).

Individual tree detection

To obtain the stem volume and biomass of individual trees using LiDAR data, individual trees initially have to be detected and the crown boundaries delineated. Watershed segmentation is a powerful partitioning tool for gray-scale images, for example CHM. Therefore, watershed segmentation is a useful method for isolating single trees from the CHM (Chen et al. 2006). In image processing, watershed segmentation is an algorithm based on the topology of the image. The distance of the gradients is interpreted as elevation information. During the successive flooding of the grey value relief, watersheds with adjacent catchment basins are constructed. This flooding process is performed on the gradient image, i.e., the basins should emerge along the edges (Soille 2003). Through watershed segmentation the edges (valleys) of each crown in the CHM can be found, and the treetop (peak) extracted within the delineated crown boundary (Fig. S4).

However, general watershed segmentation methods have some problems in that the number of individual trees may be overestimated or underestimated, because of the large height variation within their topography or smaller treetops under the crowns of the higher trees (Kwak et al. 2007). Thus, to reduce these commission and omission errors, Popescu et al. (2004) accomplished tree segmentation using the local-maxima detecting method, by adopting flexible window sizes according to the relationship between tree height and crown size. Chen et al. (2006) presented marker-controlled watershed segmentation, which performs watershed segmentation around user-specified markers in the input image, rather than the local maxima, to remove false treetops. In this study, the extended maxima transformation was used to reduce spurious treetops (commission errors) because of the row the CHM computed without filtering LiDAR returns (Fig. S3b). The CHM was segmented for individual crown delineations using the watershed segmentation method after processing the extended maxima transformation. Details of the delineation of individual tree crowns are described in Kwak et al. (2007).

Relationship between stem volume and CGV

Chen et al. (2007) suggested that the stem volume can be estimated from the CGV because the stem volume is proportional to the CGV, as proposed by Enquist (2002), who found the allometric relationships DBH $\propto M^{3/8}$and $H \propto M^{1/4}$, where M is the plant mass and H the tree height. Assuming that the plant is filled with an approximately constant tissue density across sizes, the plant mass, M, is proportional to CGV (West et al. 1999; Enquist 2002). Therefore, the relationship between stem volume and CGV was determined using Eq. 1:

$$V \propto \mathrm{DBH}^2 * H \propto M^{\frac{3}{4}} * M^{\frac{1}{4}} \propto \mathrm{CGV} \quad (1)$$

There is a biological basis for application of this allometric equation over part of a canopy: most terrestrial plants have a transport system that moves water, minerals, and nutrients through the plant body via plant tissues, for example xylem and phloem (Chen et al. 2007). To support the maintenance and growth of leaves and branches within any specific part of the canopy, there are corresponding conducting tubes in the stem for transporting water and nutrients (West et al. 1999), which correspond to a portion of the stem volume. Therefore, the canopy geometric volume can be related to the stem volume and biomass on the scale of a portion of an individual tree (Chen et al. 2007). On the basis of such relationships, the stem volume was estimated using three classes that were grouped according to tree density using Eq. 2. The coefficient, α, was estimated by linear regression analysis using the field-derived stem volume calculated from the tree height, and DBH and CGV computed via the crown height and crown width, respectively. The crown height was calculated as the difference between tree height and crown base height.

$$\text{Stem Volume} = \alpha \times \text{CGV} \quad (2)$$

Estimation of field-derived stem volume and CGV

The field-derived stem volume in comparison with the CGV was calculated from the field-derived tree height and DBH, using a nonlinear regression function previously developed by Kim et al. (2000), as shown in Table 1. Stem volumes were computed from the corresponding class of DBH, irrespective of the tree density class.

In particular, the crown shape factor was applied, which is a symbolic approximation for visualizing the shape based on the solid geometric shape of an individual tree crown (Coder 2000) when the CGV has been estimated from the field-derived crown height and crown width (Table S2).

In this study, a fat cone shape was used as the crown shape factor, because the crown shape of Korean Pine corresponds to type S7 (Fig. S5). If each Korean Pine occupies a very spacious area, its crown shape can be regarded as close to a cone shape, because each crown of individual trees rarely overlapped with neighbor trees. However, the Korean Pines in this study were affected by neighbor trees, without regard to tree density class, and the edges of crowns actually overlapped and mixed with each other.

Throughout the processing, field-derived stem volumes were estimated from the field-measured CGV, and the LiDAR-derived stem volumes could then be estimated by use of Eq. 2 and LiDAR-derived CGVs by tree density classes.

Table 1 Allometric equations by class of diameter at breast height of Korean Pine

Tree species	Class of DBH (cm)	Allometric equation
Korean pine	2–10	$SV = 0.00006730\ DBH^{1.8523}\ H^{0.9128}$
	12–20	$SV = 0.00006730\ DBH^{1.9594}\ H^{0.9632}$
	>20	$SV = 0.00006730\ DBH^{1.7566}\ H^{0.9050}$

SV stem volume, *DBH* diameter at breast height, *H* tree height

Computation of LiDAR-derived CGV

As mentioned above, the LiDAR-derived CGV must be derived from LiDAR data to compute the LiDAR-derived stem volume using Eq. 2. However, before determining the CGV, individual trees must be detected and delineated, using the method of Kwak et al. (2007). Depending on the segmented crown boundaries, the CGV can be estimated using LiDAR data (Fig. 2).

Before estimating the CGV, only crown returns have to be extracted from the total LiDAR data, because the CGV can be computed automatically at the individual tree level using the CHM generated from crown returns; the crown returns are defined as the returns reflected above the crown base height of individual trees (Kwak et al. 2007).

Riaño et al. (2004) attempted to test various clustering methods to classify the LiDAR data reflected from individual trees, for example a 3-m fixed limit, minimum Euclidean distance clustering, *k*-means clustering and expectation maximization clustering. In this study, the *k*-means algorithm was used, because it was the fastest

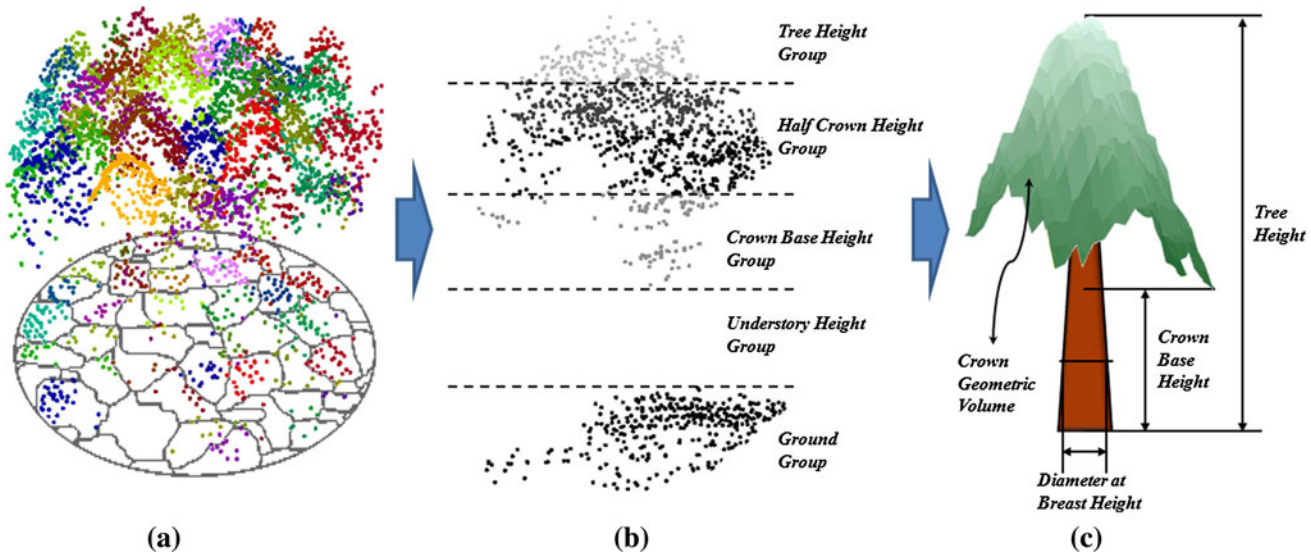

Fig. 2 **a** Classification of LiDAR data according to individual trees segmented using the Kwak et al. (2007) method. **b** Result of *k*-means clustering for LiDAR data reflected from individual tree spaces. **c** LiDAR CGV generated from crown returns

consistently working method at the individual tree level for classification of LiDAR returns.

Based on the definition of crown base height, the crown base height for the total LiDAR data was detected using the *k*-means clustering method (Fig. 2). To determine the crown base height, the LiDAR data reflected within individual trees were classified into five *Z* values: ground, understory height, crown base height, half crown height, and tree height groups, each using *k*-means clustering, because Korean Pine stands are bi-storied, applicable to the five above-mentioned clusters. The *k*-means statistic applied here is an algorithm used to classify or group attributes or features into *k* number of groups, and uses an iterative algorithm to minimize the sum of the distances (SOD, Eq. 3) from each object (*n*) to its cluster centroid (*i*), over all clusters (MATLAB 2006).

$$\mathrm{SOD}_{i,\ldots,k} = \sum_{i}^{k} \left| \mathrm{Centroid}_{i,\ldots,k} - \mathrm{Object[n]} \right| \quad (3)$$

where $\mathrm{Centroid}_i$ is the mean of the *i*th cluster of *k* clusters and object [*n*] is an observation for a given cluster, *i*. In general, the initial points of each cluster can be selected by the user when the *k*-means is performed (MATLAB 2006). In this study, the initial point values for the clusters were obtained from the field measurement. The arithmetic process was performed through 100 iterations. Also, the cluster was treated as an error if it was too small, i.e., the percentage of laser pulses of a group had less than 1/(total number of clusters)^2 (Riaño et al. 2004). Through *k*-means processing, the mean height of points (MeanLH, mean LiDAR height) within a crown base height group was used to represent LiDAR-derived crown base heights of individual trees (Fig. 2b). Finally, crown returns above the determined crown base height were transformed according to the CHM, and CGVs then calculated using the "surface volume calculation module" of ArcInfo software (ArcGIS 2001).

Estimation of biomass

The stem biomass of individual trees was estimated using the wood basic density of coniferous trees proposed by Son et al. (2008). In South Korea, no wood basic densities have been examined at the species level (Korean Pine), but rather at the phylum level (coniferous and deciduous tree) in terms of plant taxonomy (Son et al. 2008). Therefore, the LiDAR-derived stem biomass, defined as the oven-dried weight, was computed using the wood basic density for a coniferous tree (Table S3). Specifically, the LiDAR-derived stem biomass can be computed because the green volume of Korean Pine, which is the solid volume of a wood sample when it is in equilibrium with surrounding water, was calculated from the CGV (Yu 2007).

The above-ground biomass of individual trees was computed using the BCEF, which were estimated from the ratio of the weight of the branches and leaves to that of the stem of the individual tree (Son et al. 2008). Son et al. (2008) has reported that the BCEFs of coniferous and deciduous trees were 1.29 and 1.22, respectively. Therefore, the above-ground biomass of Korean Pine was estimated on the basis of the BCEF (Table S3).

Results

Segmentation of individual trees

The accuracy of segmented individual trees was evaluated using the five categories (Table S4), after performing the extended maxima transformation according to three tree densities.

To evaluate the accuracy of the delineation, individual trees, classified into correct and satisfactory categories (Table S4), were assumed to have a one-to-one relationship with field-measured trees. The number of trees with a one-to-one relationship for high, medium, and low tree density were 33 (49.2%), 26 (70.2%), and 19 (79.2%), respectively (Table 2).

The sample site with a high tree density showed too many merged trees (omission error, 44.8%), meaning that two or more trees were merged into one tree when delineated, because of the very small distances between the trees (Fig. 3a). However, the sample sites with a medium tree density had split trees (commission error, 21.6%), meaning that one tree would be divided into two or more trees in a segmented boundary (Fig. 3b). Therefore, one tree had spurious prominences (unnecessary regional maxima in

Table 2 Results of segmenting individual trees according to classes of tree density

Class of tree density	Total no. of trees	Correct		Satisfactory		Merged		Split		Not detected	
		No.	%	No.	%	No.	%	No.	%	No.	%
High	67	8	11.9	25	37.3	30	44.8	4	6.0	0	0.0
Medium	37	17	45.9	9	24.3	2	5.4	8	21.6	1	2.7
Low	24	12	50.0	7	29.2	4	16.7	1	4.2	0	0.0

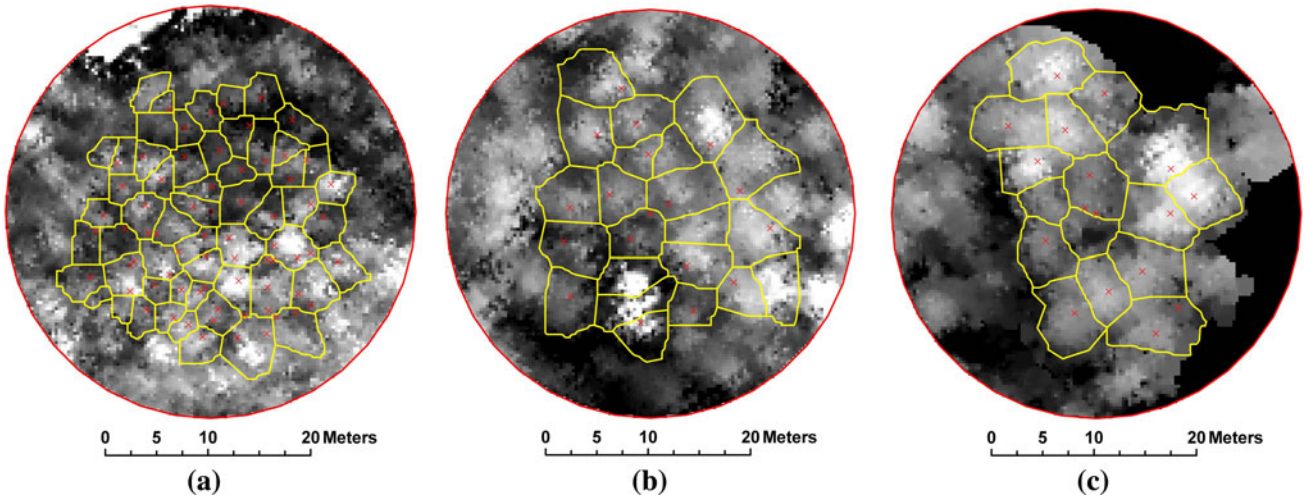

Fig. 3 Results of segmenting individual trees using the extended maxima transformation method (Kwak et al. 2007) according to tree density. "*x*" marks signify a treetop location using the field measurement. **a** High (1,340 N/ha), **b** medium (370 N/ha), **c** low (240 N/ha)

Table 3 Accuracy of the regression function generated for the crown base height

Class of tree density	Equation	R^2	RMSE (m)
High (67 N/0.05 ha)	CBH = 0.4319 × MeanLH + 8.165	0.48	0.92
Medium (37 N/0.1 ha)	CBH = 0.6952 × MeanLH + 6.842	0.51	2.35
Low (24 N/0.1 ha)	CBH = 0.6930 × MeanLH + 5.723	0.67	1.69

CBH crown base height, *MeanLH* mean laser height

image processing) on its crown surface from up-risen branches. In the case of a low tree density, fewer errors were detected than for the sample sites with high and medium tree densities, because there were fewer branches causing spurious treetops than at the other sample sites (Fig. 3c). The delineated crown boundaries were used to analyze the crown base height, crown width, and CGV of individual trees.

Estimation of crown base height

As a result of the classification of the LiDAR returns using *k*-means clustering, they were classified into five clusters: ground, understory, crown base height, half crown height, and tree height groups by classes of tree density. Afterwards, the LiDAR data were repartitioned into two groups; LiDAR returns below and above the crown base height, via the mean LiDAR height (MeanLH, mean height of crown base height group) in the crown base height group, as classified by *k*-means clustering. From LiDAR returns above crown base height, the CGVs of individual trees could be generated. In addition, linear regression analysis was carried out to determine the relationship between the LiDAR-derived and field-derived crown base heights. The coefficient of determination (R^2) and root mean square error (RMSE) were calculated to assess the accuracy of the regression analysis (Table 3). The accuracy of the LiDAR-derived crown base height also increased when the tree density decreased. This was attributed to sufficient crown returns describing the crown shape for a low tree density. The crown returns reflected from individual tree crowns in high-density plots might not be able to represent the whole crown shape, because the real crown base height was not detected under overlapping crown edges.

Estimation of crown width

DBH is the most frequent tree measurement made by foresters (Popescu 2007), and is related to several physical forest growth factors, for example tree height, crown width, tree volume, and above-ground biomass. Unfortunately, it is not directly detectable in the CHM derived from LiDAR data. Nevertheless, the DBH of individual trees can be estimated from the strong relationship with the crown width. Therefore, the crown widths were estimated using the CHM from LiDAR data for further study. As a result, the crown width was also shown to be affected by the tree density when comparing high, medium, and low tree densities, as shown in Table 4. In particular, high RMSE estimates were obtained for a high tree density. That was

Table 4 Accuracy of the regression function generated for the crown width

Class of tree density	Equation	R^2	RMSE (m)
High (67 N/0.05 ha)	$CW = 0.9448 \times CW_{LiDAR} - 0.829$	0.49	1.11
Medium (37 N/0.1 ha)	$CW = 0.9472 \times CW_{LiDAR} - 0.363$	0.54	0.86
Low (24 N/0.1 ha)	$CW = 1.0512 \times CW_{LiDAR} - 0.315$	0.61	0.63

CW crown width

Table 5 Accuracy of the regression function generated for the crown geometric volume

Class of tree density	Equation	R^2	RMSE (m^3)
High (67 N/0.05 ha)	$CGV = 1.313 \times CGV_{LiDAR} + 33.213$	0.36	40.30
Medium (37 N/0.1 ha)	$CGV = 0.500 \times CGV_{LiDAR} + 39.313$	0.52	23.73
Low (24 N/0.1 ha)	$CGV = 0.520 \times CGV_{LiDAR} + 18.851$	0.57	54.40

CGV crown geometric volume

Table 6 Accuracy assessment of the regression function generated from the field-derived stem volume and crown geometric volume

Class of tree density	Coefficient	Estimate	SE	*T* statistics	*P* value	RMSE
High (67 N/0.05 ha)	α	0.0065	0.00039	16.78	1.32×10^{-18}	0.13
Medium (37 N/0.1 ha)	α	0.0149	0.00044	34.21	6.32×10^{-28}	0.18
Low (24 N/0.1 ha)	α	0.0124	0.00058	21.28	1.56×10^{-17}	0.23

attributed to the crown width being strongly related to the crown overlapping effect according to the tree density.

Estimation of CGV

Our first approach to estimate the stem volume and biomass was based on Eq. 2. The CGV was directly derived using the CHM. However, the estimated CGV was much lower than the field-derived CGV, because the volume calculation minus the volume of overlapping crown edges was performed. In particular, the CGV was very low at high tree density sites, because the ratio of overlapping crown edges of individual trees was relatively high compared with when overlapping occurred at a low tree density site. Therefore, linear regression analysis was performed, and then corrected CGV computed using the equations in Table 5. The coefficients of determination for model fitting and evaluation were 0.36, 0.25, and 0.57 for high, medium, and low tree density sites, respectively. The problem with the tree density was also revealed by this analysis. Data for high tree density sites affected by significant crown overlapping had quite low accuracy, whereas the accuracy of data for low tree density site slightly influenced by crown overlapping was relatively high. Thereafter, the calibrated LiDAR-derived CGVs using the equations in Table 5 were used to estimate individual tree stem volumes.

Estimation of stem volume and above-ground biomass

In Eq. 2, coefficient α was estimated by linear regression analysis using field-measured stem volumes and CGVs (Table 6). Each α was estimated as 0.0065, 0.0149, and 0.0124 for high, medium, and low tree density sites, respectively. *P* values were also very low—under 95% confidence limits—and root mean square errors were also relatively low. Therefore, the coefficient α was demonstrated to be a meaningful statistic.

The coefficients of determination were found to be 0.43, 0.57, and 0.57 for high, medium, and low tree densities, respectively. However, in the case of high tree density sites, the stem volume and CGV were distributed evenly, as shown in Fig. 4a; thus, the accuracy was relatively low compared with the other sites.

With regressed equations, the LiDAR-derived stem volumes were estimated using LiDAR-derived CGVs according to classes of tree density. Field-derived and LiDAR-derived stem volumes were then compared with each other. As a result, with a low tree density, the coefficient of determination had the highest value; whereas high tree density sites had the lowest accuracy (Fig. 5). A high tree density disturbed the accurate estimation of the LiDAR-derived stem volume and other growth factors. However, this accuracy was judged to be sufficient to estimate forest growth factors, such as tree height, DBH,

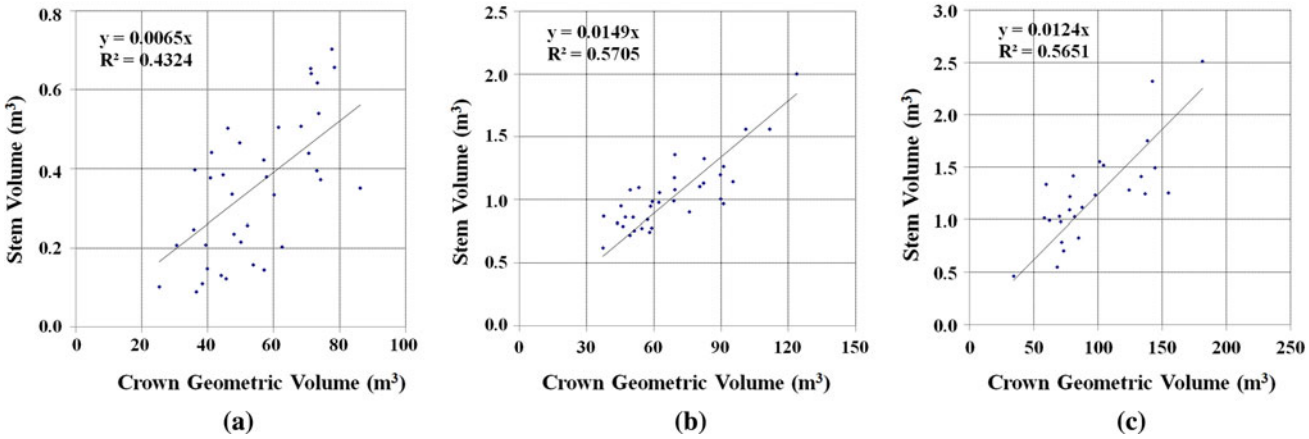

Fig. 4 These graphs show the relationship between CGVs and stem volumes using field-measured data according to tree density. The equations were developed with one-to-one relationship trees when delineated. **a** High (1,340 N/ha), **b** medium (370 N/ha), **c** low (240 N/ha)

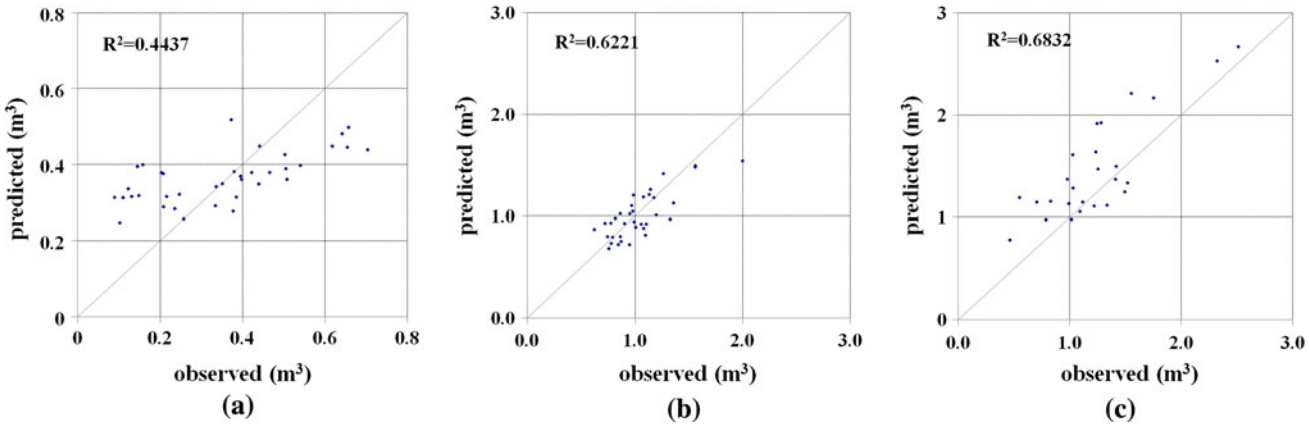

Fig. 5 These graphs show the accuracy evaluated using field data. It was observed that the lower the tree density, the higher the coefficient of determination. The equations were developed with one-to-one relationship trees when delineated. **a** High (1,340 N/ha), **b** medium (370 N/ha), **c** low (240 N/ha)

crown base height and crown width, considering the economy and labor efficiency of this method.

The LiDAR-derived stem volume was finally converted into LiDAR-derived stem and above-ground biomass (Table S3). First, the LiDAR-derived stem volume can be easily calculated using the wood basic density for coniferous trees (0.48 g/cm^3). The above-ground biomass was also computed using the biomass conversion and expansion factors for coniferous trees (BCEF, 1.29). Son et al. (2008) have found that the conversions for branches and leaves to above-ground biomass are 29 and 22% for coniferous and deciduous trees, respectively. In conclusion, above-ground biomass can be estimated by multiplying the stem volume by 0.48 and 1.29.

As shown in Table 7, the average biomass increased with decreasing tree density. The production capacity of low-density stands was better than that of high-density stands, although the errors caused by overlapping factors affected the biomass calculation. Therefore, management of the tree density can be a serious factor controlling the potential production of biomass and the capacity for carbon storage.

Discussion

Estimations of stem volume and biomass were performed in this study using airborne LiDAR data. Crown overlapping caused a major problem of underestimation of these factors; their accuracies were also ambiguous. As shown in Fig. 6, when occupied areas are supposed to be equal, the overlapping frequency and area might be small with a low tree density. However, the overlapping errors would accumulate whenever the number of trees increased, whereas the accumulated errors were relatively low for a low tree density. Increasing errors can cause other errors when estimating forest growth factors, for example tree height, DBH, crown height, and crown width. Therefore,

Table 7 Descriptive statistics of LiDAR-derived biomass

Estimated factor	Class of tree density	Max (kg)	Min (kg)	Mean (kg)	Std (kg)
Stem Biomass	High (67 N/0.05 ha)	243.82	116.44	171.68	31.27
	Medium (37 N/0.1 ha)	723.59	322.46	474.71	107.82
	Low (24 N/0.1 ha)	1,253.76	366.90	687.31	231.17
Above-ground Biomass	High (67 N/0.05 ha)	314.53	150.21	221.47	40.34
	Medium (37 N/0.1 ha)	933.43	415.98	612.37	139.09
	Low (24 N/0.1 ha)	1,617.36	473.31	886.63	298.21

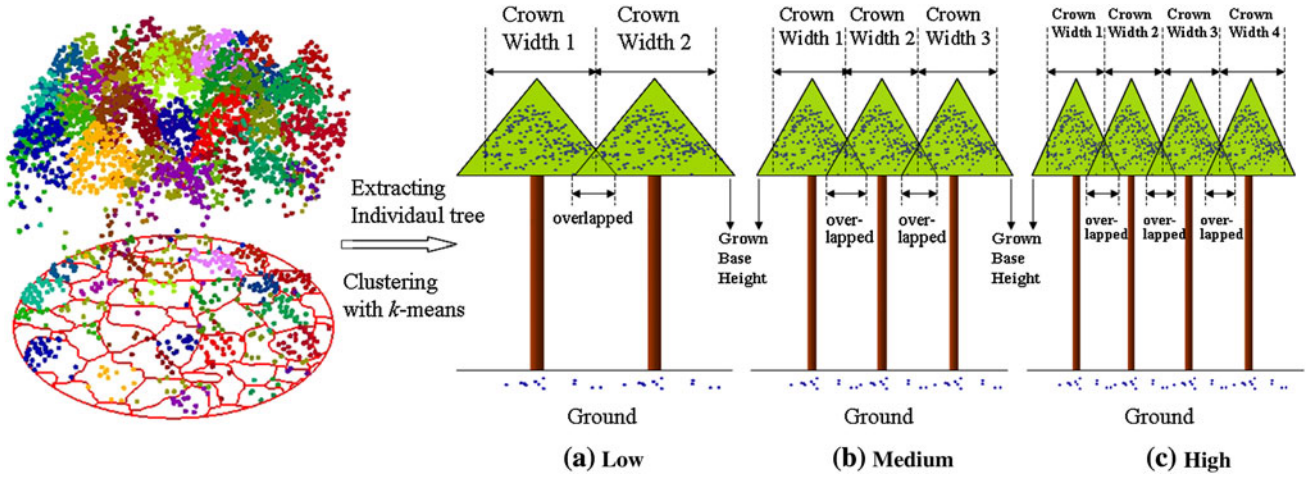

Fig. 6 The relatively overlapped area of a crown edge increases according to the tree density, because of the reduced crown width with decreasing growing space. Therefore, it is easy for LiDAR-derived growth factors to be underestimated compared with field measurements

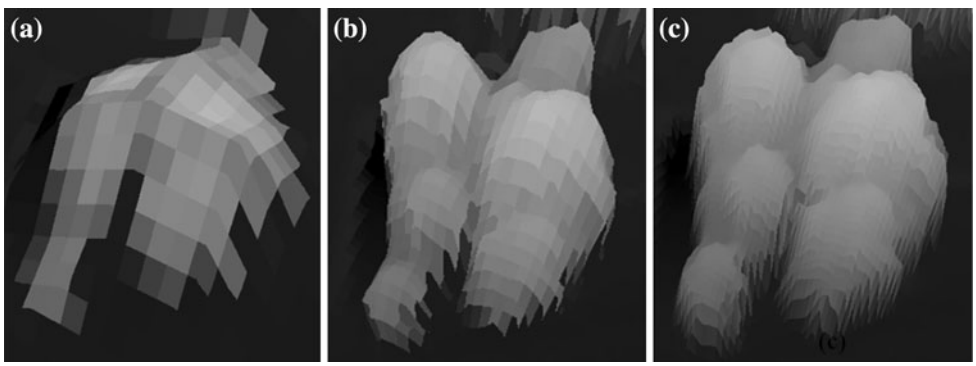

Fig. 7 These figures show how detailed crown height models can be depicted according to the point density of LiDAR data. **a–c** are the CHMs generated from low, medium, and several LiDAR points, respectively (Lim 2007). **a** Low point density. Cell size = 1.5 m × 1.5 m. **b** Mid point density. Cell size = 0.5 m × 0.5 m. **c** High point density. Cell size = 0.25 m × 0.25 m

modeling such factors according to the tree density of a target stand must be considered in future studies.

Another problem is the point density of LiDAR data. Even though the accuracy of this research was acceptable, the CHM might not accurately describe the shape of an individual tree crown because of the lack of representative LiDAR points with a low point density (Fig. 7). Moreover, the laser points used in this work had an across-track average distance of 2.0 m between each line whereas the along-track distance had an average of 1.0 m. The across-track distance affects the resolution of the CHM, because this depends on the interval between the laser points (Wehr and Lohr 1999). If the point density is higher and the across-track interval made sufficiently narrow, a better result can be expected.

In this study, the above-ground biomass was roughly estimated using the wood basic density and BCEF for coniferous trees. As yet, no studies have estimated these factors for tree species in South Korea. Although the factors for coniferous trees were used in the estimated expansion of the stem volume, another method is available, which is to estimate biomass using the DBH (Son et al.

2008). As a new method, the DBH has to be derived from LiDAR data based on individual trees. Coefficients for DBH by tree species have already been prepared and verified by Son et al. (2008). The DBH can be directly estimated from the crown width via modeling, even if the DBH is a tree dimension not directly visible on CHMs derived from airborne LiDAR data. Therefore, more accurate results would be expected if this method is applied in future studies.

Conclusion

The main objective of this research was to explore the feasibility of using small-footprint LiDAR data, with automated processing methods, to estimate the stem volume and biomass according to the tree density of individual trees (high: 1,340 N/ha, medium: 370 N/ha, low: 240 N/ha). In the case of high tree density stands, all accuracies of the estimated factors were lower than for other sites, because overlapping errors accumulate for increasing numbers of trees whereas accumulated errors are relatively low for a low tree density. Such errors can cause another error in estimating forest growth factors, for example tree height, DBH, crown height, and crown width. Therefore, it is realistically possible to use LiDAR data to estimate forest growth factors and verify the stem volume and biomass for low and medium tree densities, even if its application is difficult for dense forest stands, as evaluated in this study. Therefore, future studies for the modeling of such factors must consider the tree density of the target stand. In addition, the point density of the LiDAR data influences the accuracy of the estimated forest growth factors when the points are distributed systematically, or the point density is insufficient to describe individual tree crown shapes. If such error-causing problems can be corrected, more accurate results would be expected for extracting forest growth factors using LiDAR data. Therefore, such LiDAR-derived factors have great potential for effective application as important variables for predicting micro meteorology in forest stands or climate changes over a broad area.

Acknowledgment This study was carried out with the support of "Forest Science and Technology Projects (Project No. S120909L010130)" provided by Korea Forest Service.

References

ArcGIS (2001) Help document in program. Environmental Systems Research Institute (ESRI), United States of America

Bortolot ZJ, Wynne RH (2005) Estimating forest biomass using small footprint LiDAR data: an individual tree-based approach that incorporates training data. Photogramm Remote Sens 59:342–360

Boudreau J, Nelson RF, Margolis HA, Beaudoin A, Guindon L, Kimes DS (2008) Regional aboveground forest biomass using airborne and spaceborne LiDAR in Québec. Remote Sens Environ 112:3876–3890

Brandtberg T, Warner TA, Landenberger RE, McGraw JB (2003) Detection and analysis of individual leaf-off tree crowns in small footprint, high sampling density LiDAR data from eastern deciduous forest in North America. Remote Sens Environ 85:290–303

Chen Q, Baldocchi D, Gong P, Kelly M (2006) Delineating individual trees in a Savanna Woodland using small footprint LiDAR data. Photogramm Eng Remote Sens 72:923–932

Chen Q, Gong P, Baldocchi D, Tian YQ (2007) Estimating basal area and stem volume for individual trees from LiDAR data. Photogramm Eng Remote Sens 73:1355–1365

Coder KD (2000) Crown shape factor & volumes. Tree biomechanics series of University of Georgia 11:1–5

Drake JB, Dubayah RO, Clark DB, Knox RG, Blair JB, Hofton MA, Chazdon RL, Weishampel JF, Prince S (2002) Estimation of tropical forest structural characteristics using large-footprint LiDAR. Remote Sens Environ 79:305–319

Drake JB, Knox RG, Dubayah RO, Clark DB, Condit R, Blair JB, Hofton M (2003) Above-ground biomass estimation in closed canopy Neotropical forests using LiDAR remote sensing: factors affecting the generality of relationships. Glob Ecol Biogeogr 12:147–159

Enquist BJ (2002) Universal scaling in tree and vascular plant allometry: toward a general quantitative theory linking plant form and function from cells to ecosystem. Tree Physiol 22:1045–1064

Holmgren J, Nilsson M, Olsson H (2003) Estimation of tree height and stem volume on plots using airborne laser scanning. For Sci 49:419–428

Hyyppä J, Inkinen M (1999) Detecting and estimating attributes for single trees using laser scanner. Photogramm J Finl 16:27–42

Hyyppä J, Kelle O, Lehikoinen M, Inkinen M (2001) A segmentation-based method to retrieve stem volume estimates from 3-D tree height models produced by laser scanners. IEEE Trans Geosci Remote Sens 39:969–975

Kim JM, Park KS, Baek ES, Song YK, Ahn CY, Lee KH, Lee MH, Lee SY, Lee SH, Jeong YK, Jeong JH, Joo RW, Choi K, Choi MS, Song JH, Kim JW, Kim JY, Park MS, Song TY, Kim JH, Yang SI, Jang WH, Jang CS (2000) Forest & forestry technique. Korea Forest Service, Daejeon, South Korea

Kubo M, Nishikawa S, Yamamoto E, Muramoto K (2007) Identification of individual tree crowns from satellite image and image-to-map rectification. In: Geoscience and remote sensing symposium, 2007. IGARSS IEEE 2007 international, July 23–28 2007, pp 1905–1908

Kwak DA, Lee WK, Lee JH, Biging GS, Gong P (2007) Detection of individual trees and estimation of tree height using LiDAR data. J For Res 12:425–434

Leckie D, Gougeon F, Hill D, Quinn R, Armstrong L, Shreenan R (2003) Combined high-density LiDAR and multispectral imagery for individual tree crown analysis. Can J Remote Sens 29:633–649

Lee JK, Hwang CS, Jung SH (2003) Analysis of accuracy for the control points using the GPS continuous stations. Korean Soc Civil Eng J 23:401–409

Lefsky MA, Cohen WB, Acker SA, Parker GG, Spies TA, Harding D (1999a) LiDAR remote sensing of the canopy structure and biophysical properties of Douglas-fir western hemlock forests. Remote Sens Environ 70:339–361

Lefsky MA, Harding D, Cohen WB, Parker GG, Shugart HH (1999b) Surface LiDAR remote sensing of basal area and biomass in deciduous forests of Eastern Maryland, USA. Remote Sens Environ 67:83–98

Lefsky MA, Cohen WB, Spies TA (2001) An evaluation of alternative remote sensing products for forest inventory, monitoring, and mapping of Douglas-fir forests in western Oregon. Can J For Res 31:78–87

Lefsky MA, Cohen WB, Harding DJ, Parker GG, Acker SA, Gower ST (2002) LiDAR remote sensing of aboveground biomass in three biomes. Glob Ecol Biogeogr 11:393–399

Lim C (2007) Estimation of urban tree crown volume based on object-oriented approach and LiDAR data. Master's Thesis, International Institute for Geo-Information Science and Earth observation, Enschede, Netherlands, p 23

Lim KS, Treitz PM (2004) Estimation of above ground forest biomass from airborne discrete return laser scanner data using canopy-based quantile estimators. Scand J For Res 19:558–570

Lim K, Treitz P, Baldwin K, Morrison I, Green J (2003) LiDAR remote sensing of biophysical properties of tolerant northern hardwood forests. Can J Remote Sens 29:658–678

Malhi Y, Meir P, Brown S (2002) Forests, carbon and global climate. Philos Trans R Soc London A 360(1797):1567–1591

MATLAB (2006) Help document in program. Mathwork, United States of America

Means JE, Acker SA, Harding DJ, Blair JB, Lefsky MA, Cohen WB, Harmon ME, McKee WA (1999) Use of large footprint scanning airborne LiDAR to estimate forest stand characteristics in the Western Cascades of Oregon. Remote Sens Environ 67:298–308

Morsdorf F, Kötz B, Meier E, Itten KI, Allgöwer B (2005) The potential of discrete return, small footprint airborne laser scanning data for vegetation density estimation. In: Proceedings of ISPRS WG III/3, III/4, V/3 Workshop Laser scanning 2005, September 12–14, 2005, Enschede, The Netherlands

Naesset E (1997) Estimating timber volume of forest stands using airborne laser scanner data. Remote Sens Environ 61:246–253

Nelson R, Krabill W, Tonelli J (1988) Estimating forest biomass and volume using airborne laser data. Remote Sens Environ 24:247–267

Persson Å, Holmgren J, Söderman U (2002) Detecting and measuring individual trees using an airborne laser scanner. Photogramm Eng Remote Sens 68:925–932

Popescu SC (2007) Estimating biomass of individual pine trees using airborne lidar. Biomass Bioenergy 31:646–655

Popescu SC, Wynne RH (2004) Seeing the trees in the forest: using LiDAR and multispectral data fusion with local filtering and variable window size for estimating tree height. Photogramm Eng Remote Sens 70:589–604

Popescu SC, Wynne RH, Nelson RH (2003) Measuring individual tree crown diameter with LiDAR and assessing its influence on estimating forest volume and biomass. Can J Remote Sens 29:564–577

Popescu SC, Wynne RH, Scrivani JA (2004) Fusion of small footprint LiDAR and multispectral data to estimate plot-level volume and biomass in deciduous and pine forests in Virginia, USA. For Sci 50:551–565

Riaño D, Chuvieco E, Condés S (2004) Generation of crown bulk density for Pinus sylvestris L. form lidar. Remote Sens Environ 92:345–352

Shimada M, Muhtar Q, Tadono T, Wakabayashi H (2001) Tree height estimation using an airborne L-band polarimetricinterferometric SAR. In: Geoscience and remote sensing symposium, 2001. IGARSS IEEE 2001 international 3:1430–1432

Soille P (2003) Morphological image analysis: principles and applications, 2nd edn. Springer, Berlin

Son YM, Lee KH, Park YK, Kim RH, Kwon SD (2008) Management plan for absorption and emission of green house gas in part of forest. Korea Forest Research Institute, Seoul

Tange T, Kojima K, Yagi H, Suzuki M (1994) Influence of stand density on the increment of leaf biomass in the young *Cryptomeria japonica* stand before canopy closing. Bull Tokyo Univ For 92:37–44

Van Aardt JAN (2004) An object-oriented approach to forest volume- and above-ground biomass-by-type modeling using small-footprint lidar data for segmentation, estimation, and classification. Ph.D. dissertation, Virginia Polytechnic Institute and State University, Blacksburg, Virginia, p 23

Wehr A, Lohr U (1999) Airborne laser scanning-an introduction and overview. ISPRS J Photogramm Remote Sens 54:68–82

West GB, Brown JH, Enquist BJ (1999) A general model for the structure and allometry of plant vascular system. Nature 400:664–667

Yu C (2007) Variation of wood basic density, pulp yield and other wood properties for four Eucalyptus clones in Stora Enso Guangxi (China) plantation. Master's Thesis, Luleå University of Technology, Sweden, p 16